MULTI-SCALE COMPUTATION IN HEMODYNAMICS

- Towards to the noninvasive simulation of cardiovascular blood flow -

Hao LIU

Computer and Information Division, RIKEN
2-1, Hirosawa, Wako-shi, Saitama 351-0198 JAPAN
e-mail: hliu@postman.riken.go.jp

Abstract. Blood dynamics in cardiovascular system involve length scales in vastly different ranges, entailing dimensions from cell surface receptors on the *nm* order up to large arteries with *cm* length. Hemodynamics is of multi-scale physical phenomena but conventional theories are mostly established at the individual levels of scale. Multi-scale method can break the whole work into individual but interactive domains, making the approach practical and promising for tackling the vast scale present in hemodynamics. We have developed a multi-scale, computational method that is able to predict blood flow and pressure in the systematic arteries at any position along the vessels and to compute local flow patterns as well as wall shear stresses at any point in any vessel or organ. A one-dimensional model is established on a basis of the axisymmetric Navier-Stokes equations for flow and pressure propagation in compliant and tapering vessels. The three-dimensional model is utilized for specific vessel or organ, which is an in-house solver for the full Navier-Stokes equations and is embedded into the one-dimensional network model for the systematic arteries. Results are presented for a comprehensive study on blood flow in a human aortic arch and demonstrate that the multi-scale computation in hemodynamics provides a noninvasive simulation-based tool for medical applications.

1. Introduction

Blood dynamics in the cardiovascular system is of multi-scale physical phenomena. At different levels of scale, different objects come into view and they together reveal the phenomenon of living. For instance, atherosclerosis may be linked to the macroscopic mechanics of arteries and also to the microscopic mechanics of endothelial cell, but they are interrelated in terms of the wall shear stress.

An overall view of the hemodynamics in circulation system is schematically illustrated in Fig. 1. At the level of global circulation system with a meter-size scale, hemodynamics is characterized by the flow and pressure propagation in a multi-branching, network with compliant and tapering vessels; and the feature can be predicted efficiently using the zero or one-dimensional model based on either the lumped parameter model or the axisymmetric Navier-Stokes equations. The macro-hemodynamics at the level of *cm*-scale that usually points to some specific large vessel or organ often show a rich variety of vortical flows and separation as a result of the dynamic pulsation of the blood flow, and the richness & complexity of the geometry of vessels or organs. This blood flow characteristics can help us to understand the detailed information of the complex flow fields with applications to wall shear stress (WSS), a major factor in the onset, the development, and the outcome of the arteriosclerosis. Here, full Navier-Stokes equations need to be resolved under appropriate boundary conditions associated with flow and pressure so as to explain the feature of the time-varying WSS distribution in space and in time. Further scaling down to the level of *mm*-scale, we have a view of microcirculation in the capillaries where the mass transport of blood cells, oxygen and ADP, etc functions in nutrient and waste transport; and the meso-hemodynamics treats the blood as two-phase or multi-phase fluid, i.e., a mixture of plasma (water, proteins, enzymes, etc.) and blood cells rather than the Newtonian fluid. At the cell level of μm–scale, the micro-hemodynamics often points to the cell biomechanics that deals with the deformation and remodeling of the arterial endothelial cells under wall shear stress stimulation as well as the mass transport across the endothelium, which are of fundamental importance because it may provide important insight into understanding of arterial disease, e.g., atherogenesis. At the single molecular level of *nm*-scale, the nano-hemodynamics deals with the mechanics of a single

molecular, e.g., the platelet and the gene may play a key role, but most remain unknown. Therefore, to stack up the individual hemodynamics in forming a "whole" hemodynamics in cardiovascular system may deepen our understanding of interrelationship among the scales and hence provide a novel global view of the hemodynamics; and the computational biomechanics is capable to make the approach practical and promising for this huge milestone.

As the first step, with consideration of medical application in computation-aided diagnosis and surgery, we believe that a computational, multi-scale, macro-hemodynamic method that combines the one-dimensional modeling for global flow and pressure propagation and the three-dimensional modeling for local wall shear stress under normal physiological and abnormal conditions may be feasible by taking into account of the interrelated interactions at the levels. We have developed such a method that is able to predict blood flow and pressure in the systematic arteries at any position along the vessels and to compute local flow patterns as well as wall shear stresses at any point in any vessel or organ. A one-dimensional model is established on a basis of the axisymmetric Navier-Stokes equations for flow and pressure propagation in compliant and tapering vessels. The three-dimensional model is utilized for specific vessel or organ, which is an in-house solver for the full Navier-Stokes equations and is embedded into the one-dimensional network model for the systematic arteries. We present some preliminary results for a comprehensive study on blood flow in a human aortic arch and demonstrate that the multi-scale computation in hemodynamics provides a noninvasive simulation-based tool for cardiovascular blood flow.

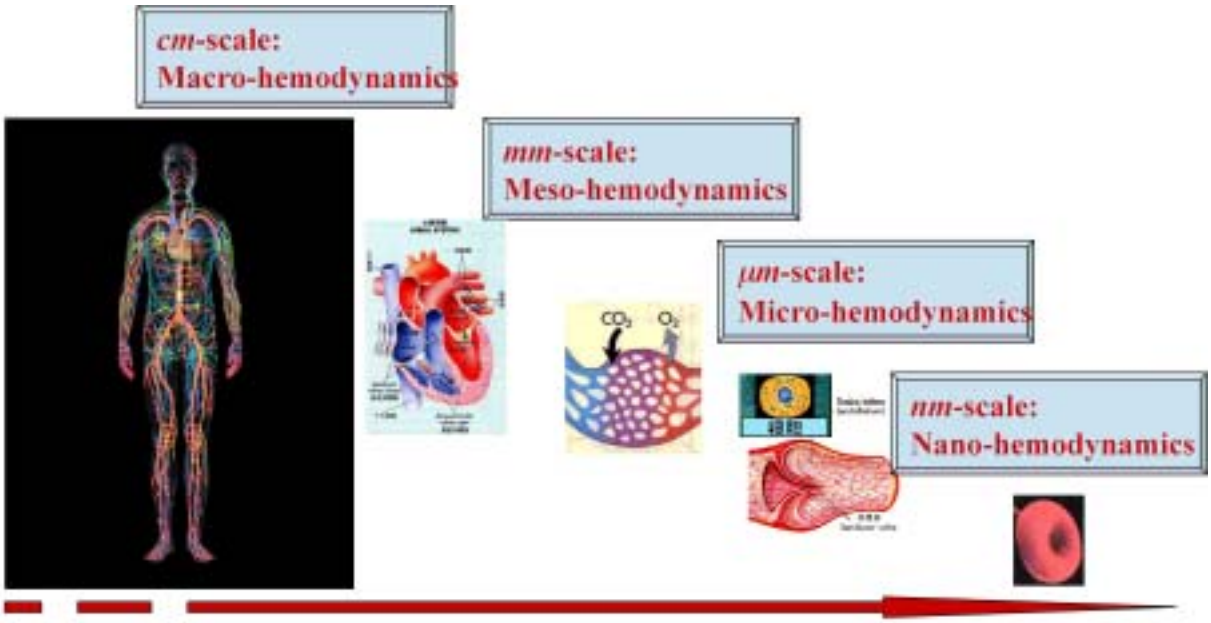

Fig. 1 Schematic diagram of multi-scale computation in hemodynamics

2. One-dimensional modeling of global flow in the systematic arteries

Following Olufsen et al. we constructed a systematic arterial tree as illustrated in Fig. 2, which is modeled as a binary tree where the geometry of the vessels may be determined from the measured medical images, e.g., MRI or based on general statistical relationships that are estimated from literature data. A typical vessel in this tree is modeled as an axisymmetric compliant cylinder; and hence computation of flow rate and pressure in the compliant vessel requires an equation of mass or volume, an equation of momentum, and an equation of state, such that,

$$\frac{\partial A}{\partial t} + \frac{\partial q}{\partial x} = 0 \quad , \tag{1}$$

$$\frac{\partial q}{\partial t}+\frac{\partial}{\partial x}\left(\frac{q^2}{A}+B\right)=-\frac{2\pi\nu qR}{\delta A}+C \quad , \tag{2}$$

$$p(x,t)-p_0=\frac{4}{3}\frac{Eh}{r_0}\left(1-\sqrt{\frac{A_0}{A}}\right) \quad , \tag{3}$$

where

$$B=\frac{4}{3}\frac{Eh}{r_0}\frac{\sqrt{A_0A}}{\rho},\ C=\frac{\partial B}{\partial x}-\frac{A}{\rho}\frac{\partial p}{\partial x} \quad ,$$

$$\frac{Eh}{r_0}=k_1\exp(k_2r_0)+k_3 \quad .$$

Here q(x,t) denotes flow rate; p(x,t) is pressure that does not vary over the cross-section; A(x,t) is area of the cross-section that corresponds to the radius R(x,t); ρ is density; ν is viscosity; and r_0 is the radius when the pressure equals to the diastole pressure $p(x,t)=p_0$. Note that δrepresents the boundary layer thickness for the large arteries, approximately 0.1cm. The vessel is assumed to taper exponentially, i.e., the equilibrium radius is $r_0(x)=r_{top}\exp(\log(r_{bot}/r_{top})x/L))$ when $p(x,t)=p_0$. The r_{top} and r_{bot} denote the inlet (top) and outlet (bottom) radii of the vessel. Note that, in order to keep the model simple, viscoelasticity is disregarded in the state equation and the relationship is derived from the linear theory of elasticity. Here, $k_1=2.00\times10^7$ g/(s^{2}cm), $k_2=-22.53$ cm^{-1}, and $k_3=8.65\times10^5$ g/(s^{2}cm) are all taken constant.

Fig. 2 A systematic arterial tree with compliant vessels

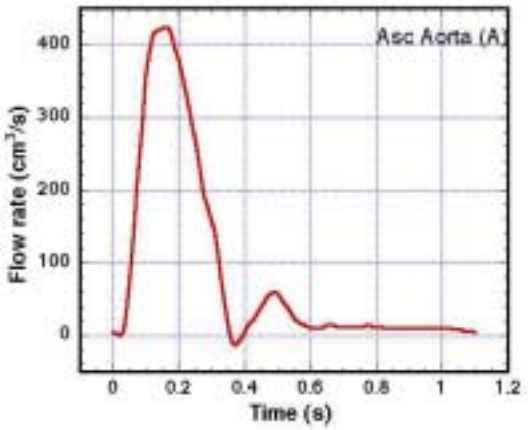

Fig. 3 MR measured flow at Asc. Aorta

With consideration of the consistency with the solutions to the full Navier-Stokes equations, the preceding governing equations are reformed in a vector form **U**, and solved in an implicit Euler scheme with a MUSCL-type 3rd-order upwind scheme for the convective terms. A delta form for the increment δ**U** is gained as,

$$\frac{\partial \mathbf{U}}{\partial t}+\frac{\partial \mathbf{F}}{\partial x}=\mathbf{S} \quad , \tag{4}$$

where

$$\mathbf{U}=\begin{bmatrix} A \\ q \end{bmatrix}, \mathbf{F}=\begin{bmatrix} q \\ \dfrac{q^2}{A}+B \end{bmatrix}, \mathbf{S}=\begin{bmatrix} 0 \\ -\dfrac{2\pi\nu qR}{\delta A}+C \end{bmatrix},$$

which is a linear system of equations and can be solved by a tri-diagonal matrix solver efficiently.

Bifurcation conditions are quite important because bifurcations represent an outflow boundary for the parent vessel and an inflow boundary for the daughter vessels. We assume that all bifurcations occur at a point and that there is no leakage so that the continuity in flow volume and the pressure leads to following conditions,

$$q_{pa}=q_{d_1}+q_{d_2}, \; p_{pa}=p_{d_1}=p_{d_2}, \tag{5}$$

where subscripts pa, d_1, and d_2 represent the parent vessel, and the two daughter vessels, respectively. At the aortic arch, the loss of energy that is expressed in terms of a loss coefficient K is introduced at the inlet of one daughter vessel with a value of K=0.75. At inlet to the arterial tree, i.e., the ascending aorta a magnetic resonance measurement of the flow is imposed as shown in Fig. 3. At outlets, a lumped parameter model by Stergiopulos et al. is employed, which is a modified windkessel model accounting for both the resistive and the compliant effects of vessels beyond the point of termination. The resulting outflow boundary condition takes the form

$$\frac{dq}{dt}=\frac{1}{R_1}\frac{dp}{dt}+\frac{p}{R_1R_2C_T}-\left(1+\frac{R_1}{R_2}\right)\frac{q}{R_1C_T}, \tag{6}$$

where $R_1+R_2=R_T$ denotes the total resistance of the termination branch, and C_T is the compliance.

3. Three-dimensional modeling of local blood flow

A PAtient-Specific Simulator (PASS) for hemodynamics that we developed (Liu, et al., 2001) has formed a foundation for the simulation-based diagnosis and surgery. The PASS is an integrated system, involving an image-based morphological model, a realistic physiological model, and a multi-block, computational mechanical model. The morphological modeling system can reconstruct an anatomic model for vessels and/or organs based on medical images of MRA, US, and CT X-ray, and generate meshes for computation. The physiological modeling is measurement-based, in which blood velocity and pressure are measured by techniques such as MRA and Doppler US. It offers boundary conditions needed by the detailed simulation through a quasi-static hydraulic model.

The basic solver is an in-house NS solver in which the incompressible, unsteady Navier-Stokes equations are discretized in a manner of finite volume method (FVM) and are solved in a time-marching manner using the pseudo-compressibility technique by adding a pseudo time derivative of pressure to the continuity equation. Since computational modeling of blood flow requires solving, in the general case, the three-dimensional transient-flow equations in deforming blood vessels the arbitrary-Lagrangian-Eulerian (ALE) description of media is employed, in which the fluid and wall domains are allowed to move to follow the distensible vessels and deforming fluid sub-domain. Here the fluid is assumed to be homogeneous, incompressible and Newtonian. The governing equations are the incompressible, unsteady Navier-Stokes equations, written in strong conservative form for momentum and mass and nondimensionalized in an integral form such that:

$$\int_{V(t)} \mathrm{St}\left(\frac{\partial \mathbf{q}}{\partial \tau}\right)dV+\mathrm{St}\frac{\partial}{\partial t}\int_{V(t)}\mathbf{Q}dV+\oint_{S(t)}\mathbf{f}\cdot\mathbf{n}\,dS=0, \tag{7}$$

where the last term $\mathbf{f}=(\mathbf{F}+\mathbf{F}_v, \mathbf{G}+\mathbf{G}_v, \mathbf{H}+\mathbf{H}_v)$ expresses the net flux across the cell surfaces. Other terms are defined as:

$$\mathbf{Q}=\begin{bmatrix} u \\ v \\ w \\ 0 \end{bmatrix} \mathbf{q}=\begin{bmatrix} u \\ v \\ w \\ p \end{bmatrix} \mathbf{F}=\begin{bmatrix} u^2+p \\ uv \\ uw \\ \beta u \end{bmatrix} \mathbf{G}=\begin{bmatrix} vu \\ v^2+p \\ vw \\ \beta v \end{bmatrix} \mathbf{H}=\begin{bmatrix} wu \\ wv \\ w^2+p \\ \beta w \end{bmatrix}, \tag{8}$$

$$\mathbf{F_v} = -\frac{1}{\mathrm{Re}}\begin{bmatrix} 2u_x \\ u_y + v_x \\ u_z + w_x \\ 0 \end{bmatrix} \quad \mathbf{G_v} = -\frac{1}{\mathrm{Re}}\begin{bmatrix} v_x + u_y \\ 2v_y \\ v_z + w_y \\ 0 \end{bmatrix} \quad \mathbf{H_v} = -\frac{1}{\mathrm{Re}}\begin{bmatrix} w_x + u_z \\ w_y + v_z \\ 2w_z \\ 0 \end{bmatrix}.$$

In the preceding equations, p is pressure; u, v, and w are velocity components in Cartesian coordinate system, x, y, and z; t denotes physical time; τ **is** pseudo time; V(t) is the volume of a cell; S(t) is the surface of the cell; $\mathbf{n}=(n_x, n_y, n_z)$ are components of the unit outward normal vector corresponding to all the faces of a polyhedron cell. Re is Reynolds number and St is Strouhal number. Note that, in the fourth component of Eq. (8), the method of pseudo-compressibility is employed with a time derivative of pressure artificially added to the equation of continuity with a positive parameter β. Note that the term $\boldsymbol{q}$ associated with the pseudo time is designed for an inner-iteration at each physical time step, and will vanish when the divergence of velocity is driven to zero so as to satisfy the equation of continuity. Details can be found in Liu et al. 2000.

4. Coupling the 1D and 3D models: a prototype multi-scale model of aortic arch

As a prototype multi-scale hemodynamic model we have recently incorporated a recently developed 1D computational model for cardiovascular system into the PASS model. We are aiming at establishing an interactive, multi-scale model in which, not only the global one-dimensional model can provide boundary conditions for the local three-dimensional model in terms of flow rate q and pressure p, but also that the three-dimensional model with realistic geometry can be used to improve the one-dimensional model in terms of feedback of the detailed flow information such as pressure drop.

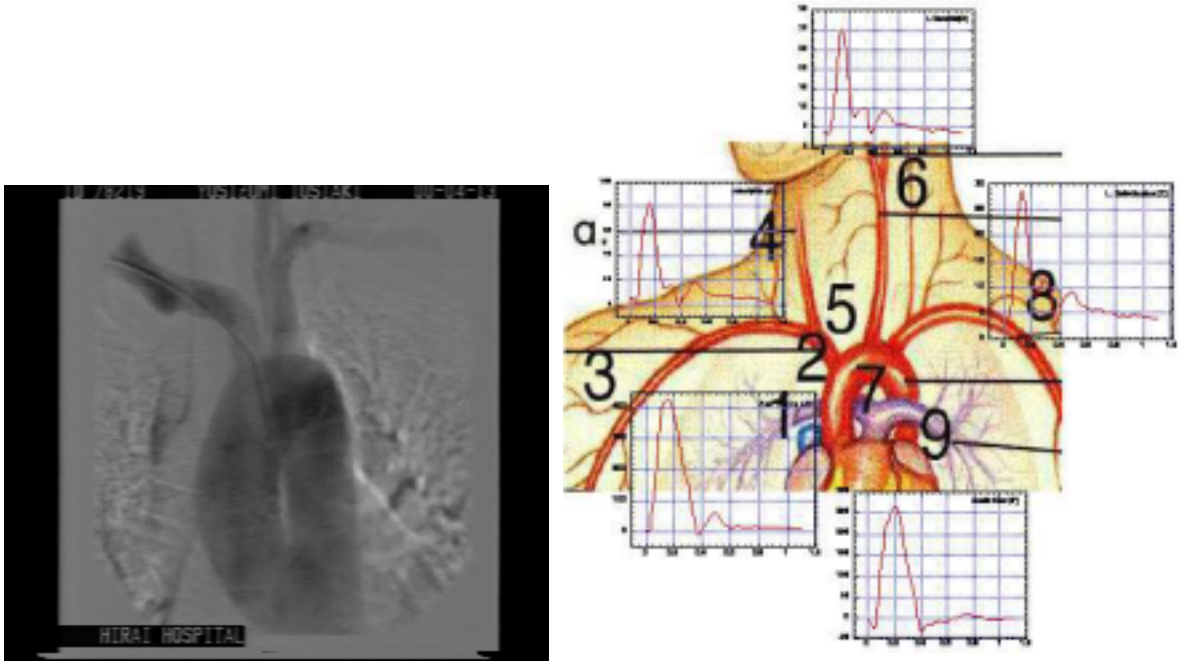

Fig. 4 A prototype multi-scale model of aortic arch aortic arch

A prototype multi-scale model of aortic arch as illustrated in Fig. 4 has been constructed; in which an idealized geometric model and a realistic anatomic model based on X-ray images as well as the magnetic resonance measurement of inflow wave at the Asc. aorta are utilized and the profiles of outflow at the Dsc. aorta, the Anonyma artery, the L. Carotid artery, and the L. Subclavian artery are

defined based on the prediction of the one-dimensional model. At inlet to the arterial tree, i.e., the Asc. aorta, the flow profile is directly imposed at the boundary with a uniform flow over the cross-section; but at each outlet three-dimensional velocity profiles are determined on a basis of the predicted flow profiles in a manner of Womersley solution and are imposed at the end of a virtual outlet region connecting to the real outlet boundary.

5. Results and discussions

Conventional computational efforts in hemodynamics mainly focus on the influence of morphology or geometry of vessel on the local flow patterns as well as the wall shear stresses, and therefore they may be identified as invasive simulation of cardiovascular blood flow because highly idealized inflow and/or outflow boundary conditions are often employed rather than the realistic physiological or pathological conditions. The inflow, however, can affect the downstream flow significantly in terms of both the flow waveform and the secondary flow over the cross-section (Liu, et al. 2000). To confirm how such difference in boundary conditions affects the blood flow in large arteries, we first carried out a computation of steady flow in an aortic arch model with two bifurcations. The velocity-based boundary conditions at inlet and outlets are based on the one-dimensional model in terms of flow rate and pressure. An extensive study is carried out to investigate how the ratio of flow rates among the outlets affects the flows in the aorta model as shown in Fig. 4, in which the color denotes the pressure decreasing from red to blue. Given a flow rate ratio between the descending aorta and the bifurcations of 7/3, the computed flow in both the aorta and in the Anonyma artery and the L. Subclavian artery show apparent difference compared with the case (a) where the velocities at three outlets are set free. The pressure is fixed to be zero at the outlet of descending artery and is set free at both outlets of anonym a. and L. Subclavian a.. Obvious discrepancy is observed in both velocity and pressure distributions.

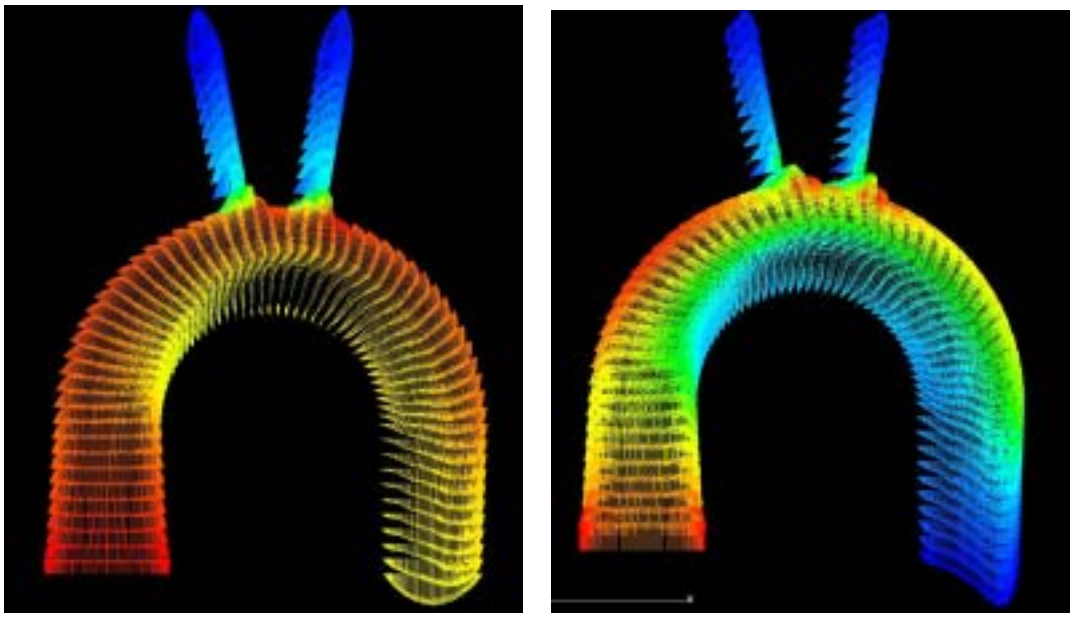

a. 1D model-based b. Free BCs for pressure

Fig. 4 Comparison of flow patterns between two boundary conditions: a. 1D model-based; b. Free boundary conditions for pressure.

Then simulation of pulsatile flow in the prototype multi-scale aortic arch model as shown in Fig. 3 was conducted. Given the reference length of the diameter at Asc. aorta, 2.5cm, the top speed based on the maximum flow rate at the Asc. Aorta (Fig. 2) of approximately 87.6cm/s, the beating period of about 1.1s, the density of 1.055 g.cm3, and the viscosity of 0.049 g/(cm3), we calculated a maximum Reynolds number of 4700 and a Womersley number of 14.0 that corresponds to a Strouhal number of

0.026. The turbulence model is disregarded in this computation and the fluid is assumed to be laminar throughout the complete beating cycle. Fig. 5 shows the flow patterns at four instants (a. Mid-systole; b. End-systole; c. Mid-Diastole; d. End-diastole) in a cycle in a form of velocity vector, in which the magnitude of the speed decreases from red to blue. The coupling of the 1D and 3D models goes well at both inlet and outlets; and the fluid is observed flowing smoothly throughout all the outlets. The Chimera-based interpolation of velocities and pressures at the bifurcation also works well.

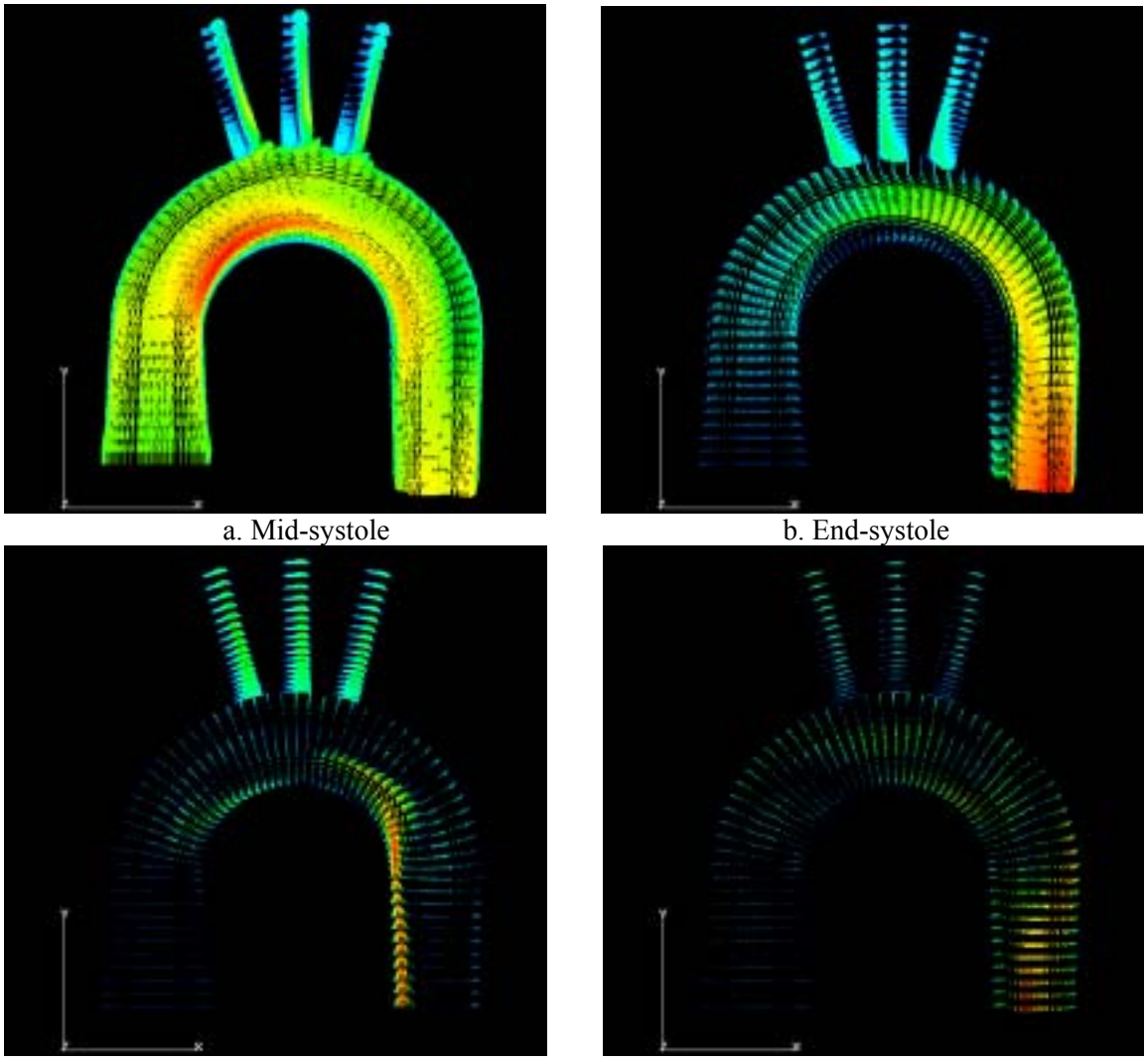

a. Mid-systole b. End-systole

c. Mid-diastole d. End-diastole

Fig. 5 Flow patterns in an aortic arch model: a. Mid-systole; b. End-systole; c. Mid-diastole; d. End-diastole.

As detected in our previous studies, the core flow in the aortic arch throughout the beating cycle shows complex vortical flow patterns quite similar with the MRA results by Kilner et al. (1993), that a primary core flow accelerates steadily at early systole (a), but substantially migrates to the outer side wall with the bifurcations, flowing through the arch somehow in a spiral way when the inflow turns to decrease against an adverse pressure gradient (b); and eventually breaks down into many vortices in a 2D structure during the diastole (c-d). However, the flow patterns at the interfaces among the aorta and the three arteries as well as around the corner do show obvious discrepancy. At the bifurcations, strong vortical flows are observed rushing into the three arteries at early systole but intense reversed flows are detected at late-systole. At the inner side of the descending aorta, a large separated region is observed steadily from the late systole to the end of the diastole.

6. Conclusion

A prototype, multi-scale, computational hemodynamic model is presented and discussed. Applications to human aortic arch has demonstrated its feasibility in medical applications of the computation-based diagnosis and surgery; and with this novel multi-scale computational method in hemodynamics the noninvasive simulation of cardiovascular blood flow would become possible.

Reference

1) N. Stergiopulos, D. F. Young, and T. R. Rogge (1992) Computer simulation of arterial flow with applications to arterial and aortic stenoses, *J. Biomechanics*, **25** (12), pp. 1477-1488.
2) P. J. Kilner, et al. (1993) Helical and retrograde secondary flow patterns in the aortic arch studied by three-directional magnetic resonance velocity mapping, *Circulation*, **88** (5), Part 1, 2235-2247.
3) L. Zabielski, et al. (1998) Unsteady blood flow in a helically symmetric pipe, *J Fluid Mech* **370**, 321-345.
4) H. Liu and T. Yamaguchi (2000) Waveform dependence of pulsatile flow in a stenosed channel, ASME *J. Biomech. Eng.*, **123**, *pp*. 88-96.
5) M. S. Olufsen, C. S. Peskin, W. Y. Kim, E. M. Pedersen, A. Nadim, and J. Larson (2000) Numerical simulation and experimental validation of blood flow in arteries with structured-tree outflow conditions, Annals of Biomedical Engineering, **28**, *pp*. 1281-1299.
6) H. Liu, (2001) Global computational modeling of cardiovascular blood flow, *Proceedings of RIKEN Symposium-Computational Biomechanics*-, RIKEN.